NOAA Technical Memorandum ERL GLERL-112

Seasonal Climatology of Surface Energy Fluxes on the Great Lakes

Brent M. Lofgren
NOAA, Great Lakes Environmental Research Laboratory, Ann Arbor, Michigan 48105

Yongchun Zhu
Cooperative Institute for Limnology and Ecosystems Research, Ann Arbor, Michigan 48109

Great Lakes Environmental Research Laboratory
Ann Arbor, MI
May 1999

NOTICE

Mention of a commercial company or product does not constitute an endorsement
by the NOAA Environmental Research Laboratories. Use of information from
this publication concerning proprietary products or the tests of such products for
publicity or advertising purposes is not authorized. This is GLERL Contribution
No. 1132.

Copies of this publications are available as PDF files and can be downloaded
from GLERL's web site: www.glerl.noaa.gov. Hard copies can be requested from
the GLERL Publications Unit, 2205 Commonwealth Blvd., Ann Arbor, MI. 48105.
pubs.glerl@noaa.gov

CONTENTS

TABLES

FIGURES

SEASONAL CLIMATOLOGY OF SURFACE ENERGY FLUXES ON THE GREAT LAKES

Brent M. Lofgren
NOAA, Great Lakes Environmental Research Laboratory, Ann Arbor, MI

Yongchun Zhu
Cooperative Institute for Limnology and Ecosystem Research, University of Michigan, Ann Arbor, MI

ABSTRACT. We estimate the seasonal cycle of latent, sensible, and net heat flux from the surface of the Great Lakes, using lake surface temperatures derived from the NOAA/AVHRR satellite instrument, along with meteorological data from surface station observations. Several well-known features are evident. Among these are very high outgoing fluxes of latent and sensible heat during the late fall and early winter, which drive strong cooling of the lakes, and greater seasonal variation of surface temperature and fluxes in shallower waters. Due to strong static stability of the overlying atmospheric boundary layer during the spring, both the magnitude and the spatial variation of latent and sensible heat flux are small during the spring season, and to a lesser degree the summer. The annual cycles of latent and sensible heat flux over the Great Lakes are opposite in phase to the same fluxes over land, indicating a large exchange of energy via atmospheric advection between the lake and land surfaces. A major weakness of the method used here is that heat fluxes are calculated on the basis of an ice-free surface, making the derived fluxes for January through March suspect.

1. INTRODUCTION

The surface temperature of the Great Lakes is part of a feedback loop constituting the lakes' energy budget. While the lake surface temperatures influence the sensible, latent, and thermal infrared heat fluxes, the lake surface temperature is itself affected by the same fluxes. Subsurface temperatures also come into play through diffusive and convective exchange of heat with the surface.

Latent heat flux associated with evaporation is the link between the heat and water budgets. It plays a role in determining the lake level and outflow from each of the Great Lakes. The heat and moisture fluxes from the Great Lakes are crucial in determining the lakes' influence on the atmosphere overlying and surrounding them, potentially leading to lake-effect precipitation and temperature and humidity anomalies.

The intensive field campaign of the International Field Year for the Great Lakes (Pinsak and Rodgers, 1981) has provided heat fluxes averaged over Lake Ontario, with latent and sensible heat fluxes calculated as residual quantities in the heat budget. Using a model of vertical thermal mixing in the Great Lakes combined with satellite observations of horizontal distributions of anomalies from the spatial mean temperature, K. Schneider (personal communication, 1993) estimated surface heat fluxes for one seasonal cycle.

This paper aims to provide a spatial distribution over each of the Great Lakes of the estimated latent, sensible, and net heat fluxes on a monthly climatological basis, calculated using an aerodynamic formulation of latent and sensible heat fluxes applied directly to satellite-derived lake surface temperatures and adjusted station-observed meteorology. Section 2 describes the methodology in detail. Section 3 describes the input data. The results are presented and discussed in Section 4, and conclusions are given in Section 5.

2. METHOD

The Great Lakes' heat fluxes are calculated using the same method used by Croley (1989). The basic equations for evaporation and sensible heat flux are similar:

$$H = -C_p \rho U_* \theta_* \tag{1}$$

$$LE = -L\rho U_* q_* \tag{2}$$

where H is sensible heat flux, C_p is the heat capacity of air at constant pressure, L is the latent heat per unit of evaporation, E is evaporation, ρ is air density (assumed constant at 1.216×10^{-3} kg m^{-3}), U_* is frictional velocity, θ_* is frictional temperature, and q_* is the frictional mixing ratio. The product LE is the latent heat flux.

The frictional velocity, temperature, and mixing ratio in the above equations are calculated as follows:

$$U_* = Uk[ln(z/z_0) - S_1]^{-1} \tag{3}$$

$$\theta_* = (\theta_a - \theta_w)k[ln(z/z_0) - S_2]^{-1} \tag{4}$$

$$q_* = (q_a - q_w)k[ln(z/z_0) - S_2]^{-1} \tag{5}$$

where U is the wind speed at the reference height, k is von Kármán's constant, z is the reference height, z_0 is the roughness length, S_1 and S_2 are stability-dependent adjustments to the fluxes, θ_a is the potential temperature of the air at the reference height, θ_w is the potential temperature of the water surface, q_a is the water vapor mixing ratio at the reference height, and q_w is the saturation mixing ratio at the temperature of the water surface. In practice, the *in situ* temperatures are used in place of potential temperatures. Since the reference height is taken as only eight meters, the discrepancy in taking the difference between the *in situ* temperatures at the surface and reference height versus the potential temperatures is less than 0.1 K.

Following Panofsky (1963) and Businger (1966), the stability dependence of S_1 and S_2 is defined by:

$$S_1 = 2ln\{[1 + (1 - a_1 z/L_M)^{1/4}]/2\} + ln\{[1 + (1 - a_1 z/L_M)^{1/2}]/2\} \tag{6}$$

$$-2tan^{-1}(1 - a_1 z/L_M)^{1/4} + 1.570796 \qquad z/L_M \leq 0$$

$$= -a_2 z/L_M \qquad 0 < z/L_M < 1$$

$$= -a_2[1 + ln(z/L_M)] \qquad z/L_M \geq 1$$

$$S_2 = 2ln\{[1 + (1 - a_3 z/L_M)^{1/2}]/2\} \qquad z/L_M \leq 0 \tag{7}$$

$$= -a_2 z/L_M \qquad 0 < z/L_M < 1$$

$$= -a_2[1 + ln(z/L_M)] \qquad z/L_M \geq 1$$

where a_1, a_2, and a_3 are empirical parameters to be described later, and L_M is the Monin-Obukhov mixing length:

$$L_M = U_*^{-3} C_p \rho T/(kgH) \tag{8}$$

where T is the temperature (in Kelvins) of near-surface air and g is the gravitational acceleration rate (9.8 m s^{-2}).

The roughness length is given using the Charnock relationship:

$$z_0 = a_4 U_*^2/g \tag{9}$$

where a_4 is another empirical parameter.

The system of equations (1)-(9) is solved iteratively, because the Monin-Obukhov length and the roughness length depend on the frictional velocity and the sensible heat flux. By calibrating against the fluxes presented in Pinsak and Rodgers (1981), Quinn (1979) acquired values of $a_1 = 16$, $a_2 = 5.2$, $a_3 = 16$, and $k = 0.41$. Separate observations by Quinn (1979) gave $a_4 = 0.0101$. The constant z is taken to be eight meters, and T is given the constant value of 276.5 K for use in (8); small variability in T relative to this absolute temperature would result in minimal changes to the surface fluxes.

Data observed at stations over land are adjusted to account for the difference between the overwater conditions compared to those over land. Based on the work of Phillips and Irbe (1978), Croley (1989) derived empirical coefficients for use in the following equations:

$$U = b_0 + b_1 W + b_2 T_a + b_3 T_w \tag{10}$$

$$T = b_4 + b_5 T_a + b_6 T_w \tag{11}$$

$$D = b_7 + b_8 T_w + b_9 D_1 \tag{12}$$

where U is the overwater wind speed, W is the overland wind speed, T_a is the overland air temperature, T_w is the water surface temperature, T is the overwater air temperature, D and D_1 are the overwater and overland dew point temperatures, and $b_0, \ldots, b_9$ are empirical coefficients given in Table 1 of Croley (1989).

This paper focuses on sensible and latent heat fluxes, but also presents net heat flux:

$$Q = R_s + R_{dl} - R_{ul} - LE - H \tag{13}$$

where Q is the net heat flux into the lake surface, R_s is absorbed solar (shortwave) radiation, R_{dl} is downward longwave radiation from the atmosphere and clouds, and R_{ul} is upward longwave radiation from the surface. The solar radiation is estimated, based on observed cloud cover, by

$$R_s = (1-\alpha)[0.355 + 0.68(1-N)]Q_0 \tag{14}$$

where α is the lake surface albedo, N is the fractional cloud cover, and Q_0 is the daily average solar radiation that would be incident on a unit area normal to the Earth's surface. The downward longwave radiation is a function of the air temperature, cloud cover, and greenhouse gas concentration; water vapor is the only greenhouse gas that is treated as a variable.

$$R_{dl} = \sigma T^4 (0.53 + 0.065 e_a^{1/2})[p + (1-p)(1-N)] \tag{15}$$

where σ is the Stefan-Boltzmann constant (5.67×10^{-8} W m^{-2} K^{-4}), e_a is the water vapor pressure in the overlying air, and p is an empirical coefficient of sensitivity to cloud cover, taken here to be 1.07. The upward longwave radiation is

$$R_{ul} = \varepsilon \sigma T_w^4 \tag{16}$$

where ε is the emissivity of the water surface, taken here as 0.97.

3. INPUT DATA

This model requires both meteorological data and lake surface temperature data as input. The meteorological data are historical data collected at stations surrounding the Great Lakes (Fig. 1) and obtained from the Midwest Climate Center. These data include temperature and dew point at screen height, cloud cover, and wind speed at 10 meters above ground level. These data were transferred to a grid with 10 km spacing using an inverse-distance weighting technique. Equations (10)-(12) were then applied to adjust for overwater conditions. The dewpoint temperature was converted into water vapor mixing ratio and water vapor pressure, as appropriate for the equation in which it was being used. We used this data over the period 1992-1995. One special case was the station at Thunder Bay, Ontario (indicated by an asterisk next to its location in Fig. 1). It was found that the temperature data at Thunder Bay was severely inconsistent with that of nearby stations throughout the years 1994 and 1995. Therefore, the data from this station were discarded during those times.

The lake surface temperatures are from the Great Lakes Coastwatch program (http://coastwatch.glerl.noaa.gov). They are derived from AVHRR measurements of surface temperatures taken from the NOAA Polar Orbiting Satellites. They are available on a 2.56 km grid, but have been transferred to a 10 km grid using inverse-distance weighting from neighboring points within 10 km. While this is an unconventional method of transferring data from one grid to another, the resulting temperature field was found to match very well whether one used this kind of inverse-distance weighting, two-dimensional linear interpolation, or a nearest-neighbor scheme. The available data cover 1992-1995, although for the first three months of the year, data from 1992-1994 have been discarded because of the lack of available quality lake surface temperature data. The results for the months of January, February, and March are shown in the following section as means over 1995 only, whereas the other months are averaged over the four years 1992-1995. For this reason and because ice cover has been ignored in the calculation of heat fluxes, the fluxes presented here for the first three months of the year should be regarded with particular caution. This is especially true for Lake Erie, whose shallow depth allows ice to form there more frequently than on the other lakes.

4. RESULTS

The results are shown in Figs. 2-4 as spatial distributions of each type of heat flux, averaged over each month for the years 1992-1995, except for January, February, and March, which are averaged only over 1995. The results are also presented in Tables 1-3 in terms of spatial averages over each lake for the same quantities.

Figure 2 displays a predictable seasonal cycle of latent heat fluxes, and Table 1 has the same information as lake-wide means. Because the latent heat of evaporation, L, is nearly constant (a very weak function of water temperature), the spatial maps in Fig. 2 are nearly proportional to maps of evaporation. There are large latent heat fluxes at the beginning and end of the year, and much smaller values during the summer, even negative at times. Negative evaporation corresponds to water condensation at the surface, or may be construed as the formation of fog just above the surface that warms the water by precipitating into it. Such processes are routinely suppressed in models using aerodynamic schemes for evaporation and surface energy exchange. Although these processes are routinely suppressed in models using aerodynamic schemes for evaporation and surface energy exchange and may not be very accurately portrayed by our scheme, they are retained here. Negative evaporation tends to have very small amplitude, as it always occurs in a situation in which the atmosphere above the lake is stable.

January (Fig. 2a) has the greatest latent heat flux over most areas. This results in part from the low absolute humidity of the cold overlying air. Winter winds and static instability of the atmospheric boundary layer result in a large Monin-Obukhov mixing length (8), further enhancing the latent heat flux. The water temperature cannot dip below 0° C, but the air temperature can, with the water vapor mixing ratio dropping correspondingly. Because the air temperature remains cold, these strong latent heat fluxes diminish only slightly into February (Fig. 2b), although in the real world, they would be greatly diminished in any location where ice would form.

During March the air has warmed and moistened considerably while the lake water has cooled, leading to considerably decreased latent heat flux (Fig. 2c). This trend continues during April (Fig. 2d), and by May (Fig. 2e), most of the area of the large lakes has near zero latent heat flux. Lake Erie and shallower areas of the other lakes are exceptions to this. Their water has warmed rapidly enough to keep better pace with the air temperature, allowing them to maintain some evaporation.

Through June and July (Figs. 2f and 2g), the area of active evaporation spreads from the shorelines toward the deeper areas at the centers of the lakes. By August (Fig. 2h), most of the lakes have evaporation occurring, but it remains strongest in the shallower areas. Lake Superior, the northernmost and deepest of the Great Lakes, warms more slowly than the other lakes, and thus has the least latent heat flux throughout the summer.

The lakes tend to have their maximum surface temperature during September. Meanwhile, the air temperatures and water vapor mixing ratios are decreasing. These factors are reflected in further increases in latent heat flux during September (Fig. 2i). Although the water cools throughout the fall, the air cools and dries more rapidly, resulting in a larger gradient in water vapor mixing ratio between the lake surface and the overlying air. This increases the latent heat flux by directly increasing the magnitude of q_* as given in (5). The accompanying unstable state of the atmospheric boundary layer further increases the latent heat flux by increasing S_1 and S_2 in (3) and (5). This is evidenced by the further increases in latent heat flux during October, November, and December (Figs. 2j, 2k, and 2l). Again, Lake Erie and shallow parts of the other lakes are exceptions to this general rule. They cool more quickly and do not maintain high rates of latent heat flux into the late fall and early winter. In general, because of the lower heat capacity of the shallower parts of the Great Lakes, their temperature throughout the year is closer to the air temperature than in the deeper areas, making the amplitude of the seasonal cycle of latent heat flux smaller. Also, the phase of the annual lake temperature cycle lags the air temperature less in shallower areas, meaning that the latent heat flux's annual cycle lags by less. An additional effect on the latent heat flux is the gradient in surface temperature due to wind-forced upwelling. Prevailing northwesterly winds during the fall season lead to cooler temperatures and lower latent heat flux in the western or northern parts of the lakes.

Sensible heat fluxes are shown in Fig. 3 and Table 2. These generally follow the same trends as the latent heat flux, high in the fall and winter and much lower during the spring and summer. They have especially high winter values in deeper parts of the lakes. Like the latent heat flux, the sensible heat flux is modulated by wind-driven upwelling. From April until August, many of the sensible heat flux values are negative, indicating that the water surface is colder than the overlying air. This situation is more readily achieved than one of negative latent heat flux, which requires that the water vapor mixing ratio of the air be greater than the saturation mixing ratio at the surface water temperature. Since the air's mixing ratio must never be greater than the saturation value at the air temperature, the mixing ratio in the air will frequently be less than the saturation value at the lake surface temperature, even though the air temperature will be greater than the lake surface temperature. Additionally, air further from full saturation will require a stronger stable atmospheric boundary layer for negative latent heat flux to occur, suppressing the turbulence that helps drive evaporation.

While the sensible heat flux is less than the latent heat flux throughout most of the year, during January, February, and December, sensible heat flux (Figs. 3a, 3b, and 3l) exceeds latent heat flux (Figs. 2a, 2b, and 2l). At relatively high temperatures, the strong dependence of the saturation mixing ratio on temperature ensures that the latent heat flux from a water surface will always be greater than the sensible heat flux. However, the saturation mixing ratio is a nonlinear function of temperature and depends less on temperature at lower temperatures.

If we make some simplifying assumptions, we can estimate the temperature at which sensible heat flux switches from being less than latent heat flux to greater, i.e., the temperature at which the Bowen ratio (sensible heat flux divided by latent heat flux) equals one. Using (1), (2), (4), and (5), the Bowen ratio is

$$B = C_p(\theta_a - \theta_w)/[L(q_a - q_w)] = 1. \tag{16}$$

First we ignore the small difference between the surface and the reference height by substituting the difference in *in situ* temperatures for the difference in potential temperatures. We further assume that the air is saturated, making this the case with the lowest possible evaporation and the upper limit of temperature at which the Bowen ratio could possibly be unity. In this case,

$$B = C_p \Delta T / L \Delta q_s = 1, \tag{17}$$

where q_s is the saturation mixing ratio. Given that the saturation mixing ratio is $.61e(T)/p$, where $e(T)$ is the saturation water vapor pressure and p is the air pressure (assume 1000 mb), and in the limit of small ΔT, $B = 1$ when

$$de/dT = pC_p/.61L = .655 \text{ mb/K}. \tag{18}$$

Using a standard water vapor pressure table, this condition is satisfied at approximately 6° C. Thus, a temperature less than about 6° C taken as a mean between the water and atmosphere is a necessary, but not sufficient, condition for having a Bowen ratio greater than one over a water surface. These effects are notable on Lake Erie, where the latent heat flux peaks in September, but the sensible heat flux does not reach its peak until January.

Figure 4 shows the monthly values of net heat flux. This adds the influence of radiation to the sensible and latent heat fluxes, as in (13). According to Table 3, each lake has negative net heat flux from October through February, with additional negative numbers appearing in March on Lakes Superior and Huron, and September on Lakes Michigan and Erie. Ideally, the annual mean net heat flux over an entire lake will be very close to zero. It is no larger than 7 W m^{-2} on any of the lakes, which the authors consider quite good, considering that there is no constraint built into our calculations to guarantee this, and there is a wide variety of possible errors in the input data and flux calculation methods.

It should be noted that the annual cycle of the net heat flux is nearly in phase with those of the sensible and latent heat flux (allowing for the sign convention used in (13)), and larger in magnitude than their sum. This means that the sensible and latent heat fluxes are working in concert with the solar radiation to yield the annual cycle of water temperatures. The summertime maximum in heating of the lakes nearly corresponds with the minimum cooling due to latent and sensible heat fluxes. This constructive relationship between the phases of the solar and turbulent fluxes is opposite to the usual situation over land, where the turbulent fluxes counteract the effect of the solar radiation.

In terms of the heat budget of the atmosphere overlying the Great Lakes, the wintertime inputs of latent and sensible heat from the lakes may be partially offset by radiative loss (although this might also be offset by absorption of longwave radiation upwelling from the relatively warm water surface). However, they must be primarily compensated by net divergence of advective heat flux from the lakes, in the form of both latent and sensible heat. This means that surrounding continental regions contribute to cooling the lakes by acting as a heat sink; because of the nearby lake, the outgoing latent and sensible heat fluxes at these continental surfaces will become even weaker than they would due only to their reaction to the seasonal cycle of solar input. Conversely, during the summer, those continental regions act as a heat source for the lakes, although this relationship is weaker.

5. CONCLUSIONS

We have presented spatial distributions of latent and sensible heat flux and net heat flux for the Laurentian Great Lakes. These fluxes represent the effects of the thermal capacity of these large water bodies creating a phase lag of their temperature relative to the temperature of the overlying air. This results in strong latent and sensible heat

fluxes during the winter, when the relatively warm water and cold, dry air create a strong vertical gradient in temperature and water vapor mixing ratio, combined with strong turbulence due to instability of the atmospheric boundary layer. During the summer, the vertical temperature gradient is reversed, and sometimes the water vapor mixing ratio is also, but strong static stability of the atmospheric boundary layer suppresses turbulent fluxes.

The net fluxes are negative during the winter and positive during the summer. Our calculated fluxes also contrast sharply with the typical annual cycle over neighboring land surfaces, where net heat flux is near zero year-round and turbulent fluxes are greatest during the summer. This indicates a significant exchange of energy through atmospheric advection between the lakes and surrounding land areas.

There is no constraint built into the simulations presented here that there be an overall energy balance over the annual cycle, but the results were quite good in this respect. Another major caveat to our results is that ice was not considered as a factor in the heat flux calculations, which would particularly influence the months of January through March.

8. ACKNOWLEDGEMENTS

9. REFERENCES

Businger, J. A. Transfer of momentum and heat in the planetary boundary layer. *Proceedings of the Symposium on the Arctic Heat Budget and Atmospheric Circulation*, The RAND Corporation, Santa Monica, California, p. 305-331 (1966).

Croley, T. E., II. Verifiable evaporation modeling on the Laurentian Great Lakes. *Water Resour. Res.* 25: 781-792 (1989).

Panofsky, H. A. Determination of stress from wind and temperature measurements. *Q. J. R. Meteorol. Soc.* 89: 85-94 (1963).

Phillips, W.D., and J.G. Irbe. Land-to-lake comparison of wind, temperature, and humidity on Lake Ontario during the International Field Year for the Great Lakes (IFYGL). Rep. CLI-2-77, Atmos. Environ. Serv., Environ. Canada, Downsview, Ontario (1978).

Pinsak, A. P., and G. K. Rodgers. Energy balance. In, *IFYGL The International Field Year for the Great Lakes*, E. J. Aubert and T. L. Richards, (eds.), National Oceanic and Atmospheric Administration, Great Lakes Environmental Research Laboratory, p. 169-197 (1981).

Quinn, F. H. An improved aerodynamic evaporation technique for large lakes with application to the International Field Year for the Great Lakes. *Water Resour. Res.* 15: 935-940 (1979).

TABLES AND FIGURES

Table 1. Latent heat flux (W m^{-2}) averaged over each lake.

	Superior	Michigan	Huron	Erie	Ontario
January	69.565	68.193	50.517	49.757	53.715
February	60.794	67.528	65.114	50.488	70.823
March	34.222	21.398	21.418	11.981	14.480
April	13.358	7.799	7.169	3.924	5.242
May	0.076	0.672	1.825	8.830	1.397
June	-1.251	9.158	4.798	26.185	3.414
July	-0.857	13.510	14.034	32.364	17.119
August	9.928	34.537	33.112	62.710	39.610
September	28.497	62.816	51.687	94.802	59.508
October	34.601	59.769	48.971	84.559	49.454
November	57.732	67.113	58.400	78.560	53.179
December	64.990	57.305	51.690	62.003	53.370
Annual Mean	30.796	38.943	33.845	47.113	34.868

Table 2. Sensible heat flux (W m^{-2}) averaged over each lake.

	Superior	Michigan	Huron	Erie	Ontario
January	122.731	76.407	61.244	53.257	59.715
February	105.989	81.034	95.655	60.710	93.055
March	43.626	14.555	19.223	3.693	7.315
April	5.327	-7.123	-3.557	-8.603	6.574
May	-7.181	-9.757	-7.137	-6.343	-7.343
June	-6.338	-5.044	-4.164	-0.919	-5.278
July	-5.236	-4.456	-1.810	-1.212	-1.927
August	-1.501	1.254	2.903	5.111	3.016
September	7.843	11.429	12.268	16.226	12.727
October	17.142	16.676	16.212	21.497	15.337
November	57.618	41.099	40.100	37.940	31.015
December	82.618	57.341	55.900	51.634	53.370
Annual Mean	34.847	22.445	23.453	19.167	21.837

Table 3. Net heat flux (W m^{-2}) averaged over each lake.

	Superior	Michigan	Huron	Erie	Ontario
January	-254.844	-193.141	-141.571	-122.982	-152.092
February	-189.017	-168.479	-181.917	-112.622	-190.127
March	-17.797	13.586	-12.080	51.344	30.956
April	101.857	94.713	94.262	114.652	91.668
May	197.935	161.515	157.803	153.933	146.753
June	217.062	154.341	167.742	141.962	157.379
July	192.620	139.539	145.537	135.787	133.526
August	144.585	84.185	88.899	65.096	72.671
September	54.081	-5.958	9.966	-28.538	-5.163
October	-26.005	-62.328	-42.700	-78.630	-50.549
November	-144.521	-137.177	-113.100	-123.940	-107.011
December	-205.065	-162.397	-143.030	-141.788	-153.577
Annual	6.948	-5.836	3.592	5.250	-0.984
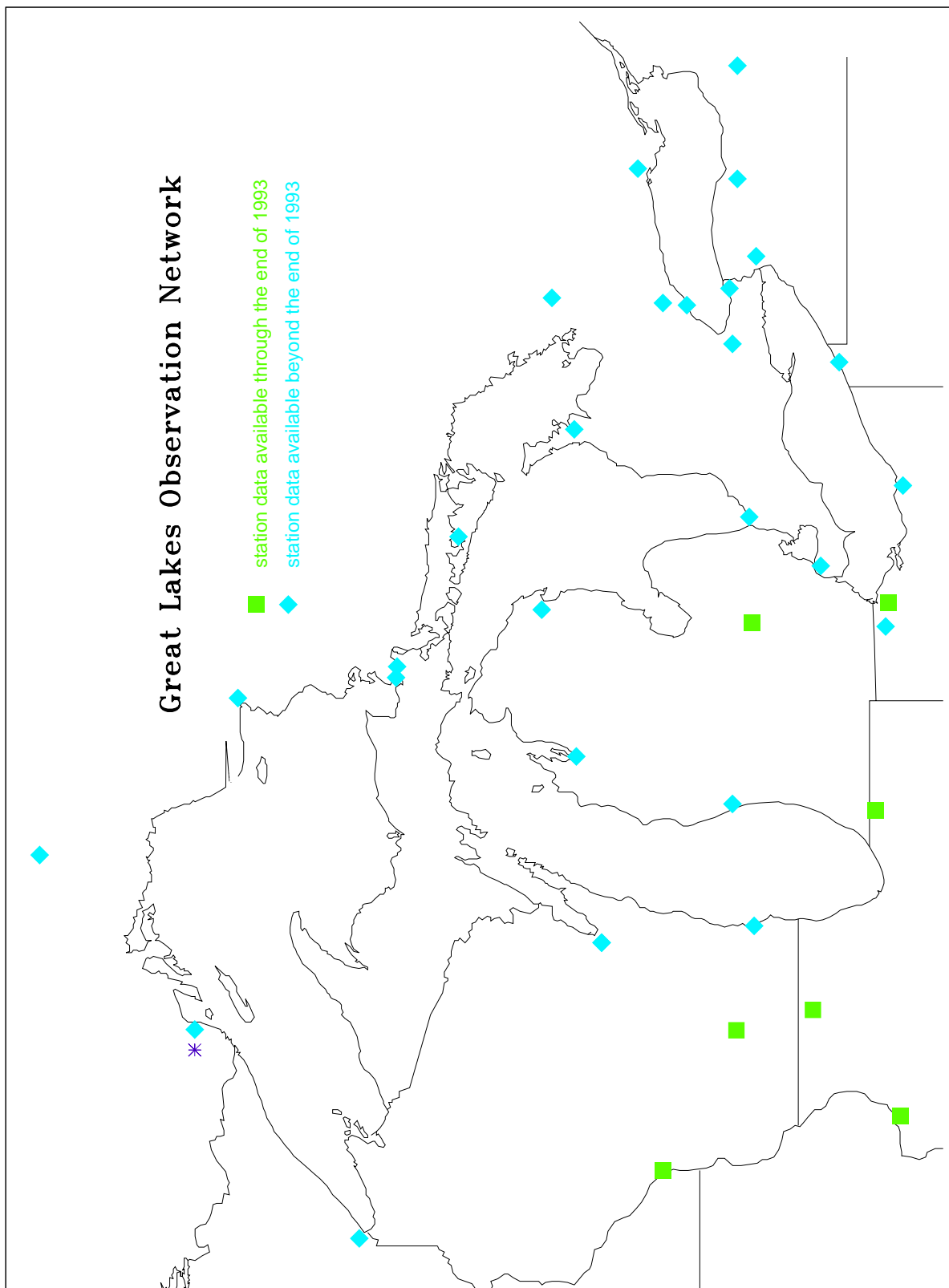
Figure 1. The distribution of stations from which meterological data are available. The blue diamonds indicate that data were available for the entire time span 1992-1995. The green squares indicate that data were available for those stations only through the end of 1993. The station at Thunder Bay, Ontario has a purple asterisk next to it to indicate special data handling because of apparent data errors (see text).
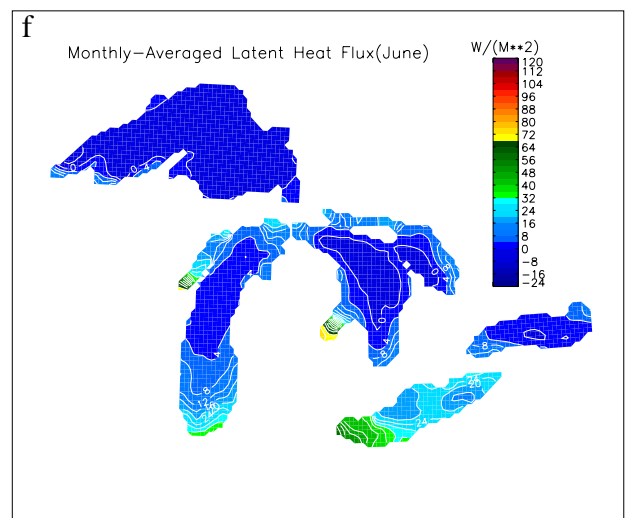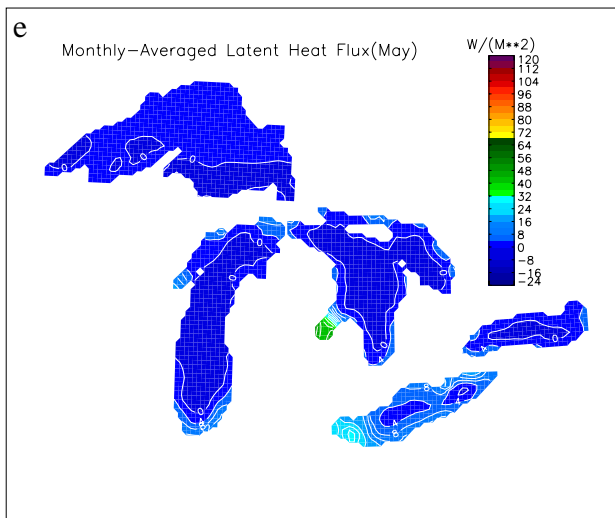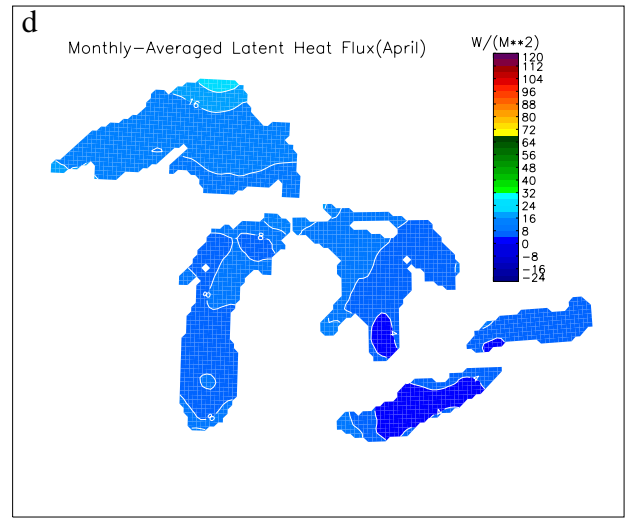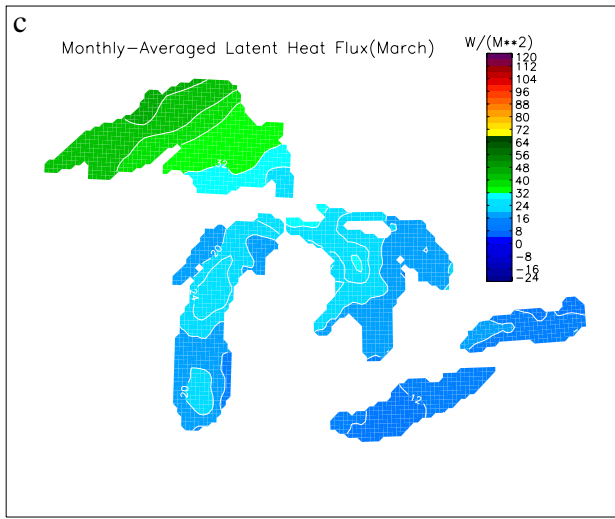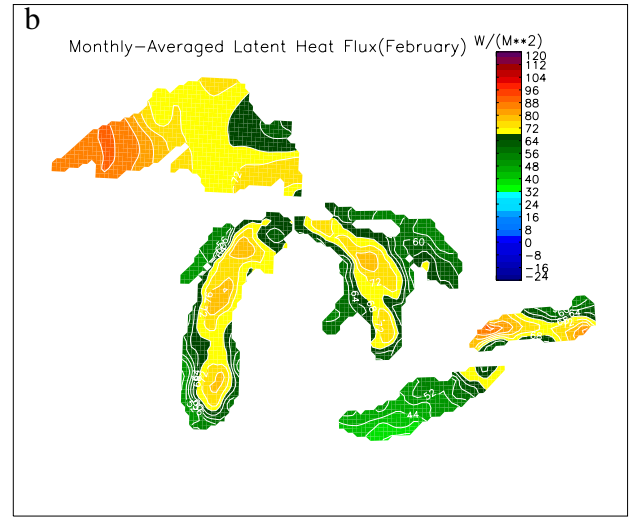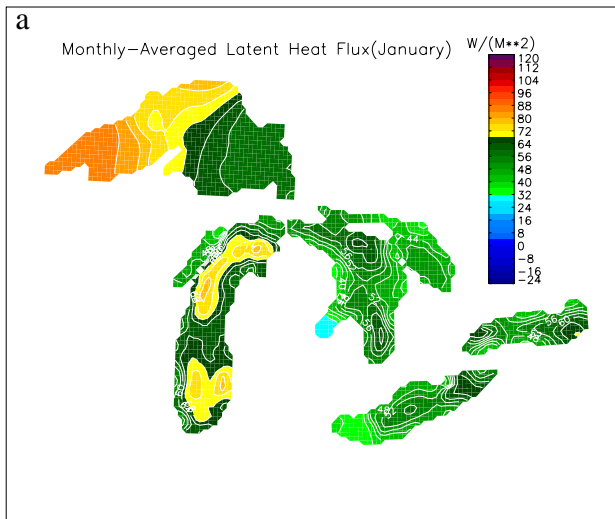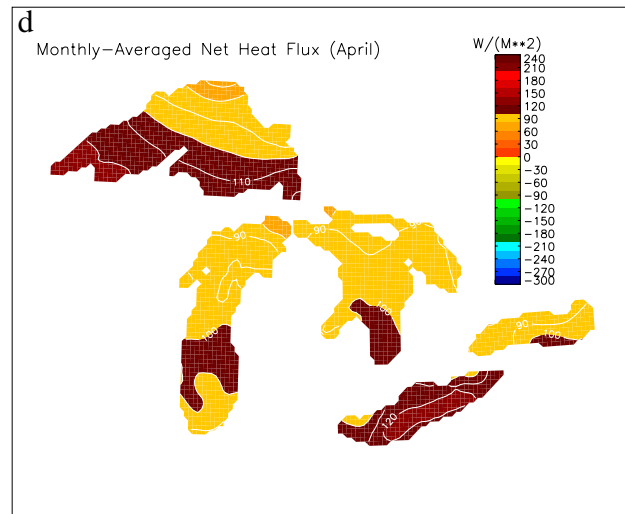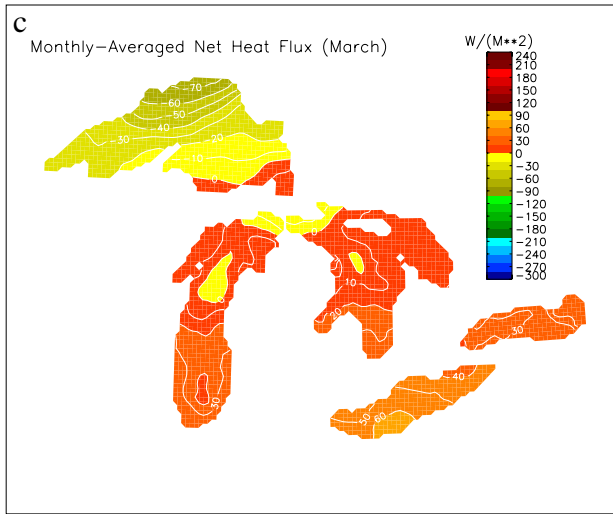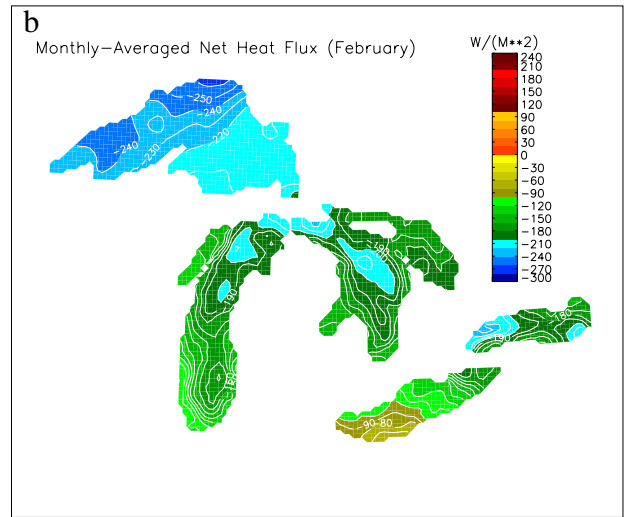
Figure 2 (a-f). The spatial distribution of latent heat flux (W m^{-2}) over the Great Lakes during the month of (a) January, (b) February, (c) March, (d) April, (e) May, (f) June, (g) July, (h) August, (i) September, (j) October, (k) November, and (l) December.

g — Monthly-Averaged Latent Heat Flux(July)

h — Monthly-Averaged Latent Heat Flux(August)

i — Monthly-Averaged Latent Heat Flux(September)

j — Monthly-Averaged Latent Heat Flux(October)

k — Monthly-Averaged Latent Heat Flux(November)

l — Monthly-Averaged Latent Heat Flux(December)
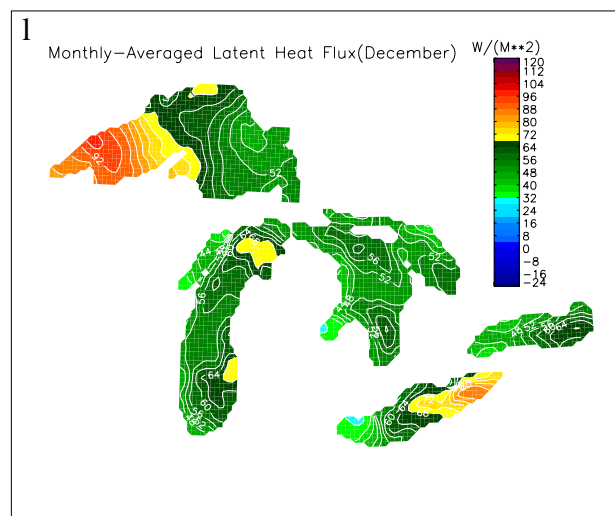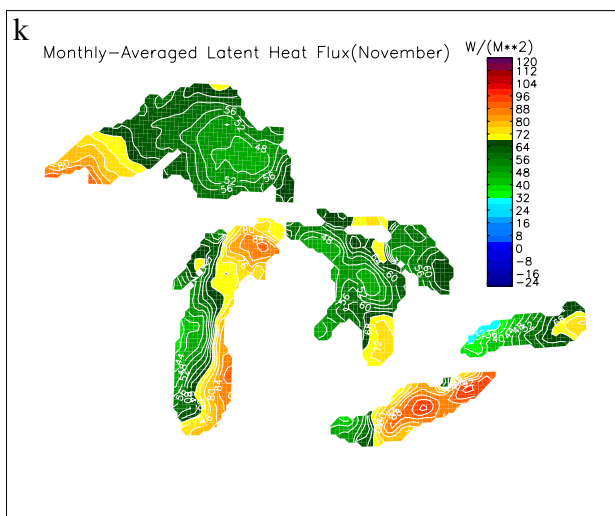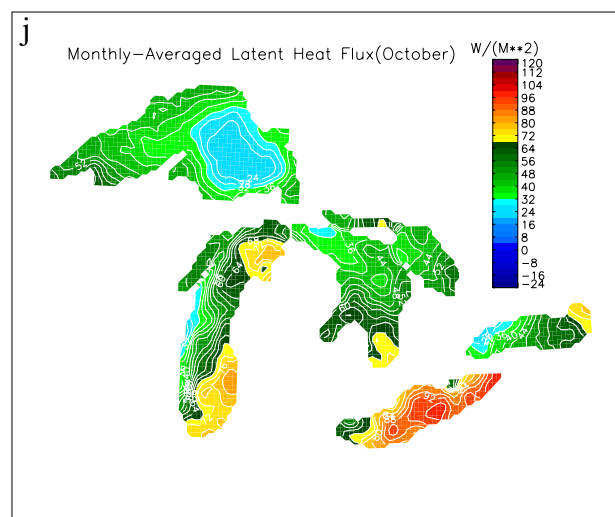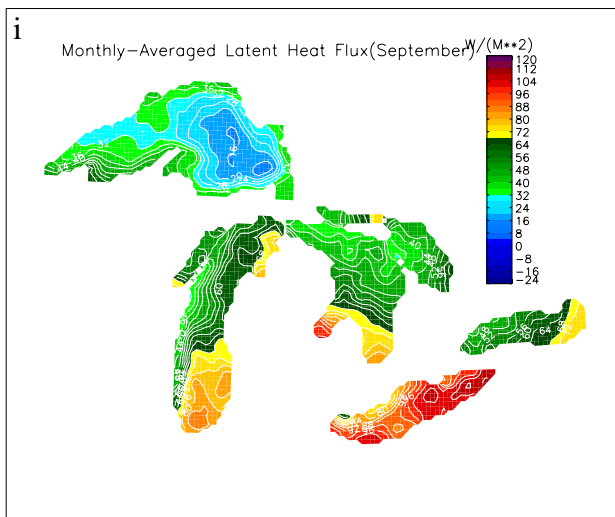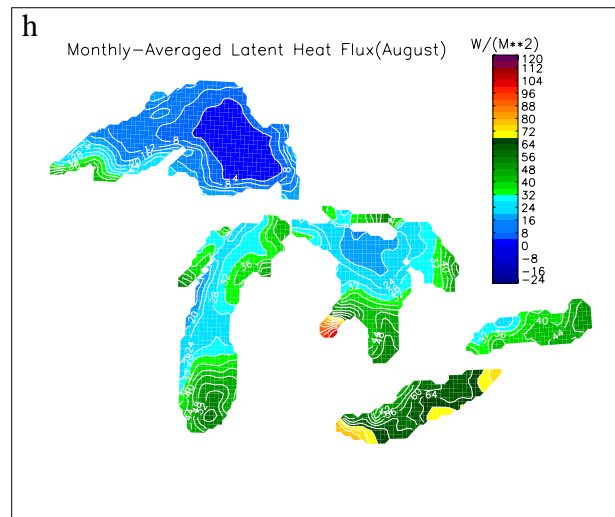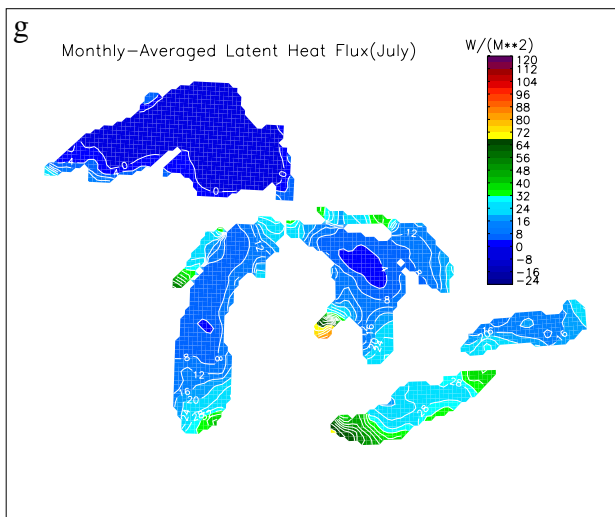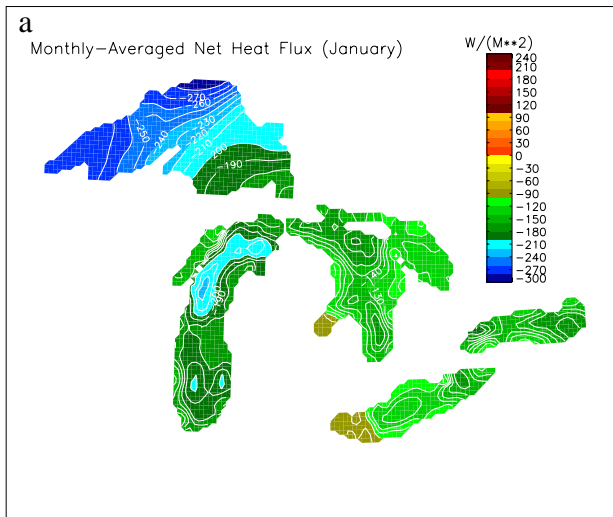
Figure 2 (g-l). Continued.
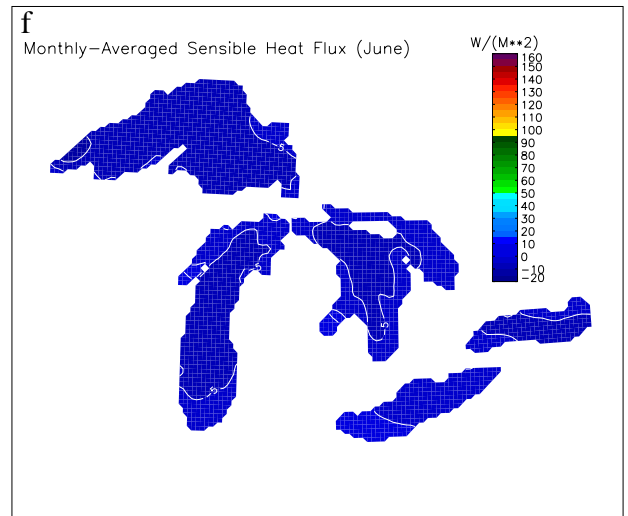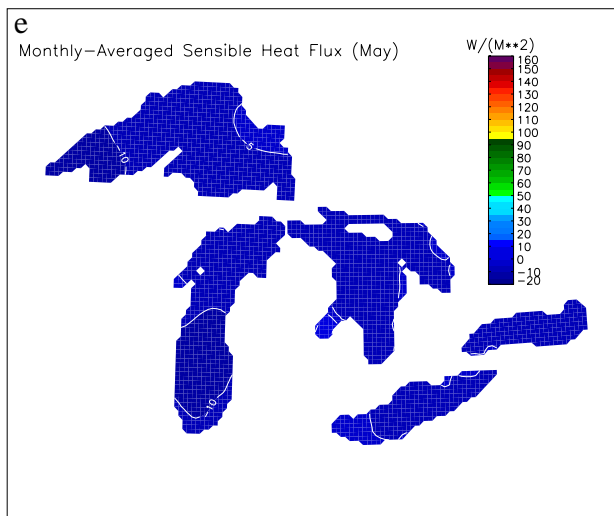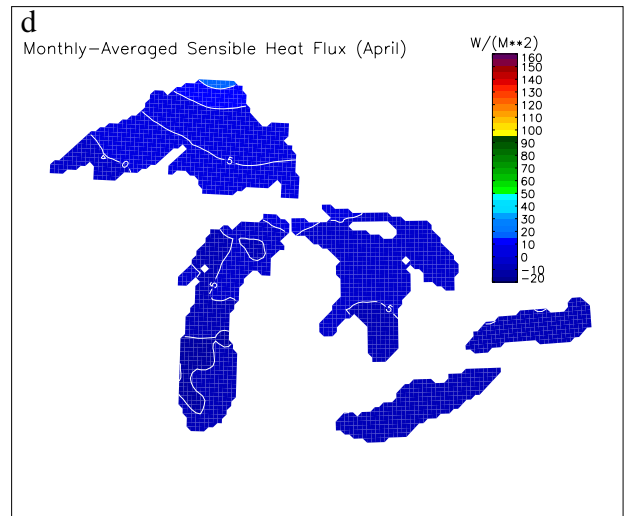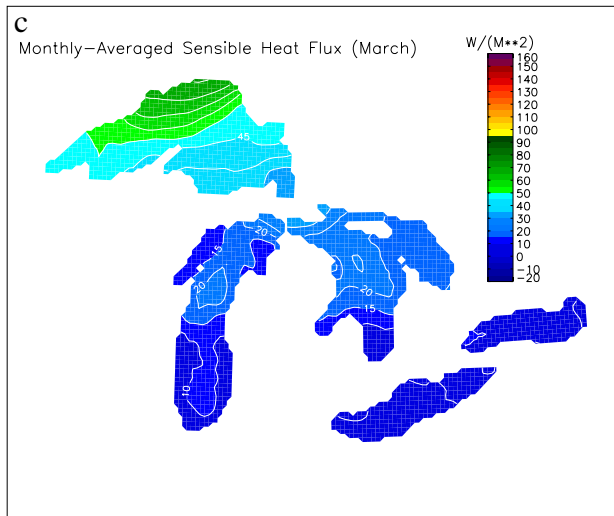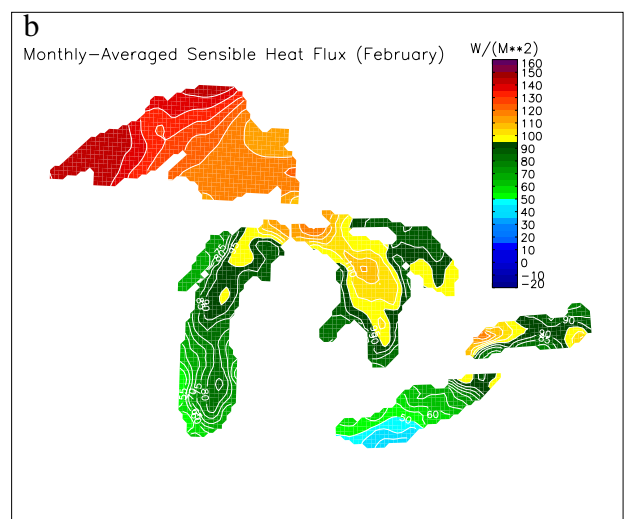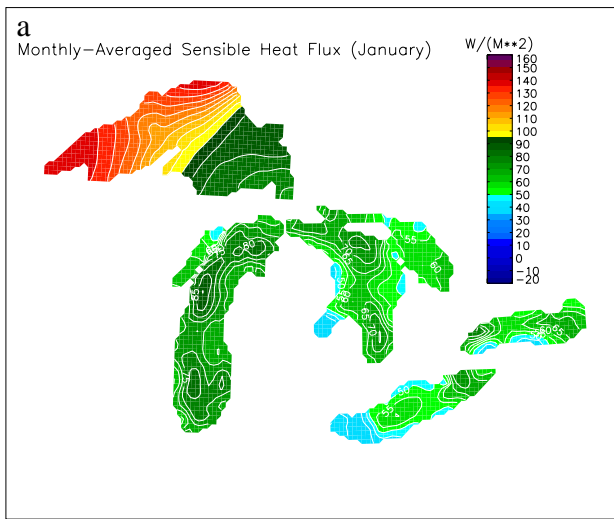
Figure 3 (a-f). The spatial distribution of sensible heat flux (W m^{-2}) over the Great Lakes, January - December.
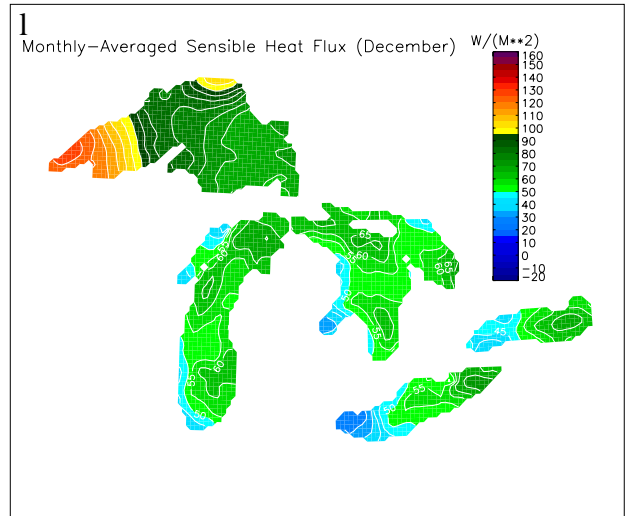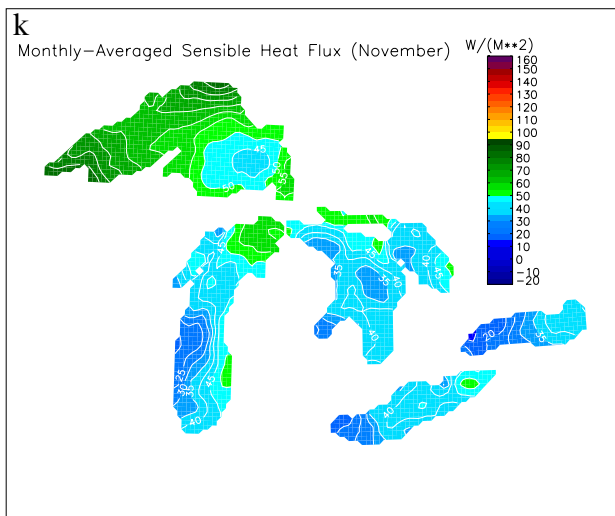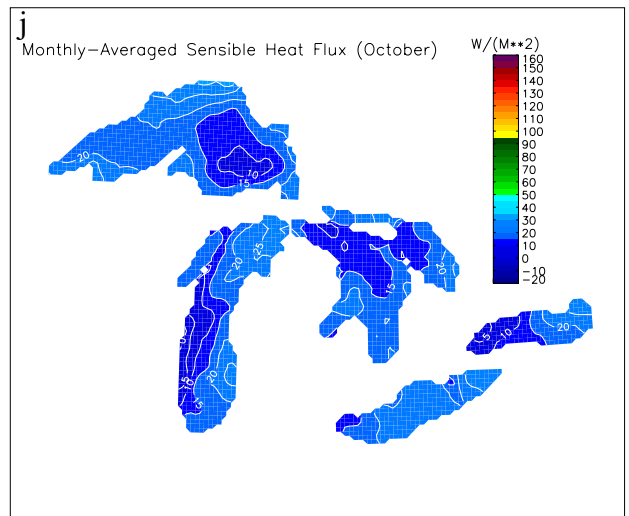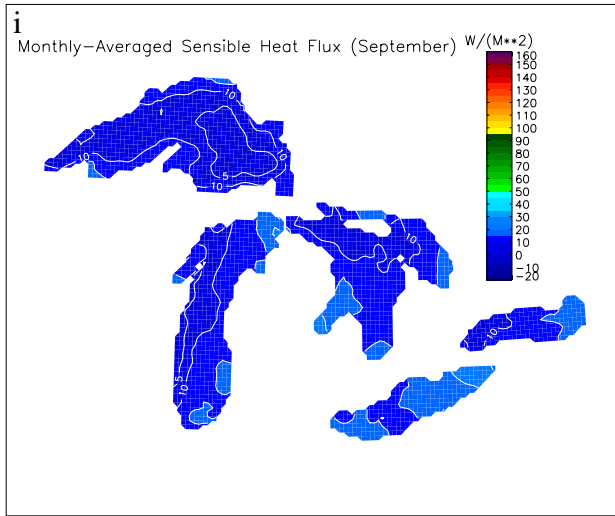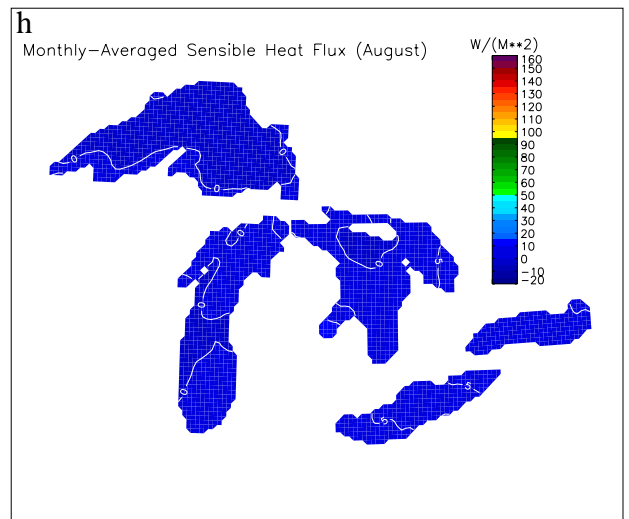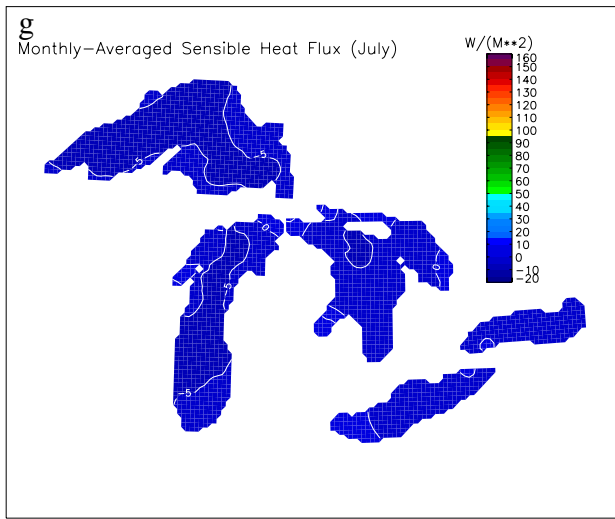
Figure 3 (g-l). Continued.

19
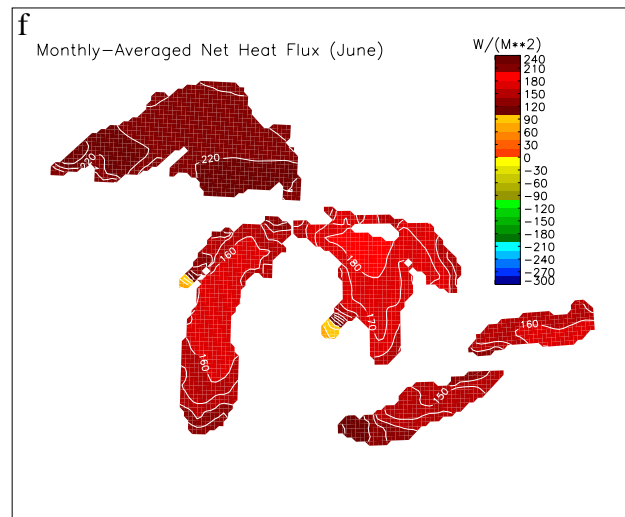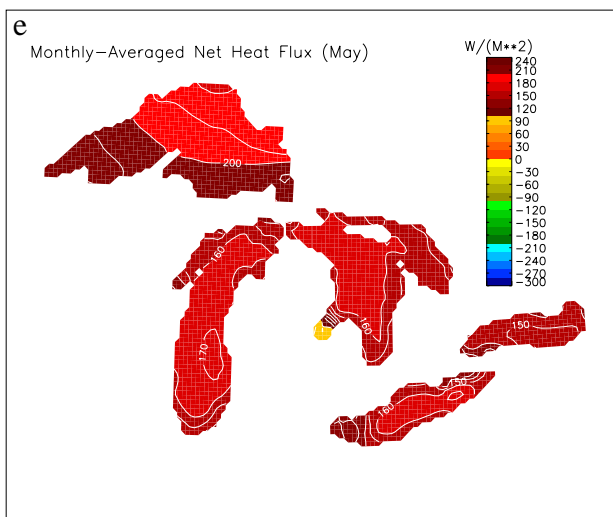
Figure 4 (a-f). The spatial distribution of net heat flux (W m^{-2}) over the Great Lakes, January - December.

g
Monthly−Averaged Net Heat Flux (July)
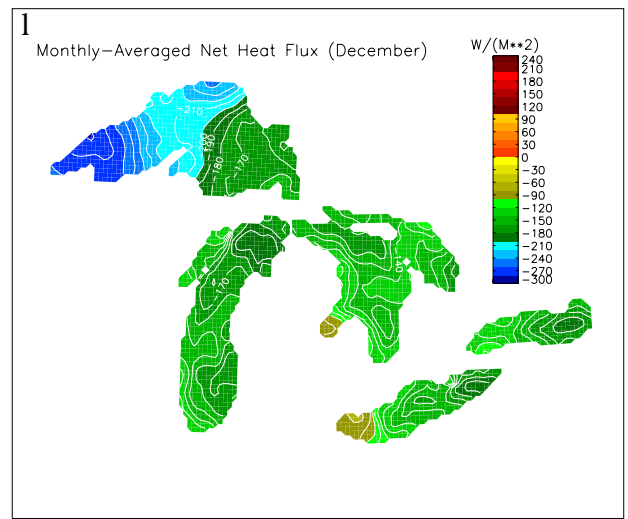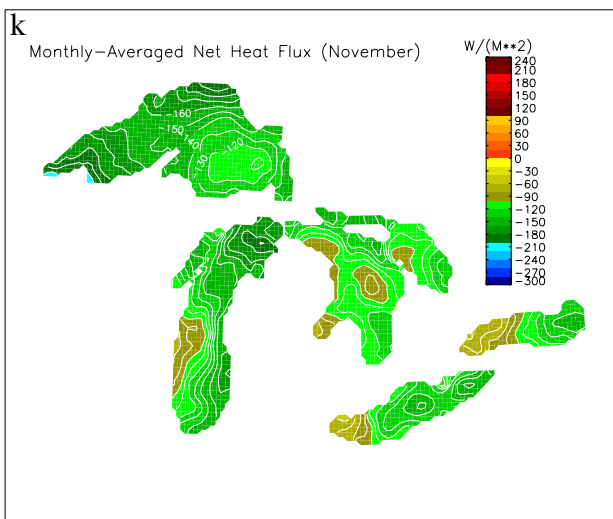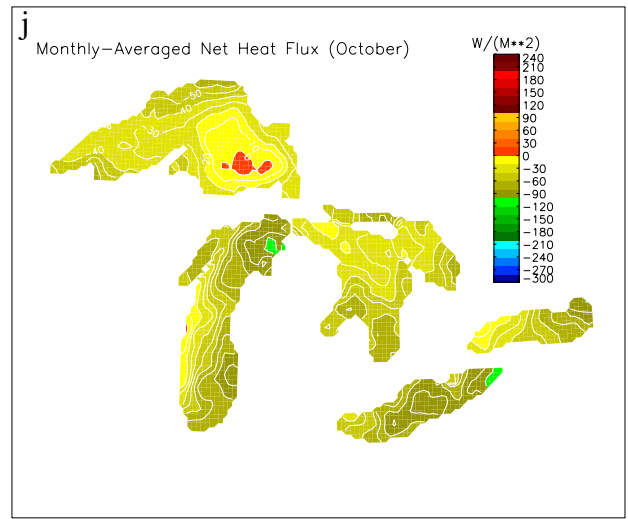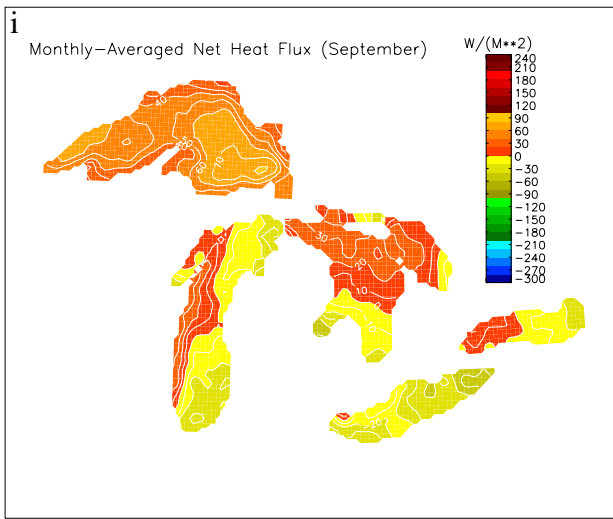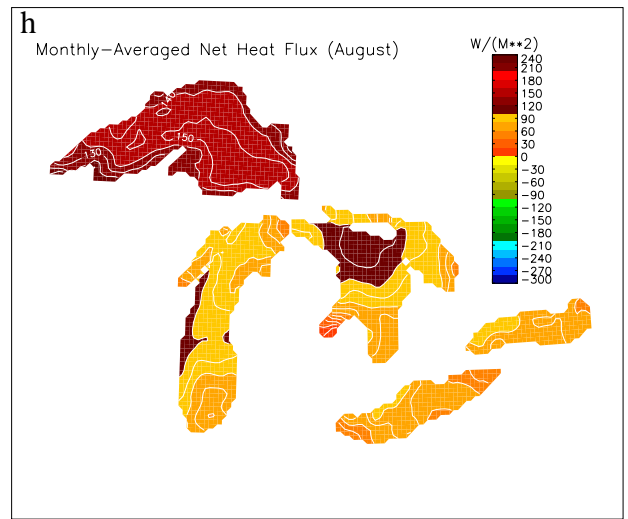
h
Monthly−Averaged Net Heat Flux (August)

i
Monthly−Averaged Net Heat Flux (September)

j
Monthly−Averaged Net Heat Flux (October)
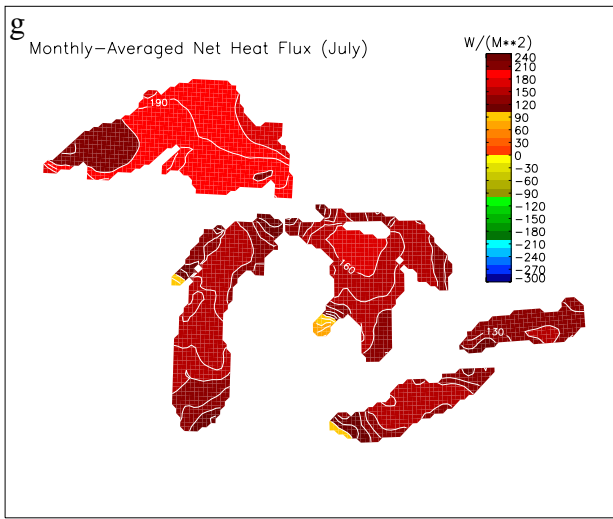
k
Monthly−Averaged Net Heat Flux (November)

l
Monthly−Averaged Net Heat Flux (December)

FIgure 4 (g-l). Continued.

21